

Design of the Angle-Resolving Electron Spectrometer Aboard the PRESET Mission

Benjamin Dyer^{1,*}, Xingzhi Cheng¹, Andrei Hanu^{1,2}, and Soo Hyun Byun¹

¹McMaster University, Canada

²Bruce Power, Canada

(*) dyerbm@mcmaster.ca

Abstract—We present a design study for the Pitch REsolving Spectrometer for Electron Transport (PRESET) mission, a CubeSat that is aimed at measuring the pitch angle density spectrum in low-Earth orbit (LEO). While a few missions have measured the pitch angle density spectrum, all have provided low resolution within the loss cone. PRESET will be capable of measuring pitch angle density of electrons with a resolution of 10 degrees or better and an energy range of 0.3-7 MeV filling gaps in both energy range and angular resolution in LEO. The spectrometer is designed to fit within a 10x10x10cm³ volume (1U) including processing electronics so it can be integrated into a 3U CubeSat to be flown in a polar LEO. To achieve a 10-degree angular resolution, the detector employs a trough shaped collimator with a pin-hole type aperture followed by a single sided silicon strip detector. Aligned coaxially with the strip detector is a stack of 4 silicon detectors. To optimize the spectrometer design, extensive Monte Carlo simulations were carried out. The collimator was optimized by adjusting total length, width and height, aperture size, collimation plate spacing and material. A balance is found between increasing the instrument's geometric factor and reducing the aperture width which directly affects the counting rate and angular resolution of the instrument, respectively. To optimize the stacking geometry of the silicon detectors, simulations were carried out by varying the number and thickness of the silicon detectors, allowing the electron energy resolution and maximum detectable electron energy to be extracted. An optimum design was deduced to accomplish an outstanding performance with a minimum of silicon detectors. Simulation results are verified using a prototype spectrometer and a commercial pulse processing system.

Keywords — silicon telescope, electron collimator, electron spectrometer, pitch angle density

I. INTRODUCTION

The Pitch REsolving Spectroscopy for Electron Transport (PRESET) mission aims to take highly resolved angular measurements of the electron pitch angle density in the Van Allen Belts. The purpose of the mission is to measure the spectrum of electrons entering the Earth's atmosphere from the Van Allen Belts due to pitch angle scattering and other transport mechanisms. To this end the Electron Spectrometer Telescope (EST) is being developed as one of two science

instruments aboard the 3U CubeSat. In this paper the design of the EST is explored through the use of Monte Carlo simulation and in lab testing.

II. BACKGROUND

The Van Allen belts are regions of radiation surrounding the Earth, composed primarily of energetic electrons or protons and a much smaller fraction of heavier ions. Measurement of the spatial and temporal particle flux distributions have always been of great interest due to the negative health effects of energetic particles, strong coupling to space weather, the existence of 'killer' electrons which can disable satellites and understanding atmospheric-ionospheric-magnetospheric interactions (AIM) [1,2]. In more recent years, the loss of Van Allen belt electrons to the upper atmosphere has been of great interest because of the potential link to global warming caused by the depletion of the northern and southern ozone layers.

Research over the past decade has shown that precipitation of medium energy electrons (MEE), that is electrons within the loss cone, leads to production of nitric (NO_x) and hydrogen oxides (HO_x). In turn, these chemicals deplete atmospheric ozone through catalytic reactions [3]. Ozone loss due to NO_x and HO_x production has been predicted using multiple models with varying results. Predictions from the Canadian Middle Atmosphere Model suggest a 60% and 80% ozone loss due to MEE in the northern and southern hemisphere, respectively [4]. Application of the Thermosphere Ionosphere Mesosphere General Circulation Model and the Solar Climate Ozone Links model, suggests a 27% and 33% decrease in ozone, respectively [5,6]. Opposing these models, analysis using the HAMMONIA model suggests no significant effect on ozone due to MEE precipitation [7]. A large factor in discrepancies between models is a lack of accurate MEE precipitation data (i.e. electron spectrum data within the loss cone) leading models to be simulated using approximated data sets with significant uncertainty [8,9].

Measurement of the pitch angle distribution began with the Energetic Particle, Composition, and Thermal Plasma (ECT) suite on board the Van Allen Probes (VAP) [10]. The VAPs launch in 2012 taking the first detailed measurement of the electron pitch angle density with a resolution of 10 degrees [11]. Two spectrometers were used for these measurements, the first being MagEIS a low energy electron spectrometer which uses a slit collimator and magnetic filtering to

determine electron energies. The energies detected range from 20keV to 4MeV across three instruments each targeting a different energy range [12]. REPT on the other hand used a cylindrical collimator and a silicon detector stack to measure electrons from 2MeV to 18MeV [11]. While the EST will measure a similar energy range to MagEIS, only a single instrument can be flown so a design more similar to the REPT will be explored.

Following the decommissioning of the VAPs, the ARASE mission began measuring the pitch angle densities of electrons in the energy range of 0.07-2 MeV using the HEP-L and HEP-H instruments. Both HEP-L and HEP-H are based on a pin-hole camera collimator design followed by a position sensitive silicon detector stack. The energies measured by the HEP-L and HEP-H detectors are 0.07-1MeV and 0.7-2MeV, respectively. The pin hole camera design allows high angular resolution measurements to be made with a resolution of 4 degrees in HEP-L and 10 degrees in HEP-H. The major disadvantage to these detector designs is a low geometric factor resulting in low counting rates. To combat this three of each instrument was flown, however this will not be possible on the PRESET mission therefore a modified approach to collimator design will be required. When at non-equatorial latitudes the loss cone increases slightly allowing an additional spectrum containing the edge and region just outside the loss cone [13,14].

The rest of this paper is structured as follows. Section III discusses methods used for simulations and how instrument performance is judged. Section IV discusses experimental verification of simulation results and comparisons between simulated and measured spectra. Section V dives into the instrument development, final design and predicted performance based on simulation data. Section VI concludes the paper and discusses next steps in development of the EST.

III. SIMULATION METHODS

The EST design was carried out using Geant4 v11.0.1. Geant4 was selected as the Monte-Carlo code of choice due to ease of parameterization and high control over data analysis. MCNP was also used in the early stages of the design to simulate idealized collimators. Thanks to MCNPs ease of use, multiple different detector geometries could be explored quickly. However, fine tuning of the detector geometry involved manually rewriting input geometry cards and processing very large PTRAC files which required significant processing time. Geant4 was therefore used for the majority of fine tuning the detector geometry and determining the detector characteristics.

The Geant4 simulations used the EM4 physics package which simulates all relevant physical processes for the EST. Since the silicon detectors can vary in thickness from 50 μm to 1500 μm , the maximum step size for all particles was reduced to 1 μm from the default of 1 mm [15]. This has the added benefit of improving accuracy of forward scattering which is a significant source of uncertainty for the detector's performance.

A. Silicon Detectors

The Electron Spectrometer Telescope (EST) design consists of two major parts, the silicon detector stack and the collimator. The size of the silicon detector stack was determined by simulating a pencil beam of electrons onto a variety of silicon stacks. The energy spectrum of the pencil beam was taken from SPENVIS using the AE-8 solar maxima model in the expected 500km polar orbit. The effectiveness of each silicon stack was judged based on full absorption of electrons up to 4 MeV. Since the upper integral bin will begin at 5 MeV or less the detector does not require high energy particles to fully deposit their energy within the detector stack as long as the instrument can differentiate between electrons and other heavier particles.

B. Collimator

The collimator was designed by describing the geometry parametrically which allowed variations in geometry to quickly be explored. The collimator's effectiveness was judged based on minimizing the number of particles that scattered one or more times before entering the silicon stack, the overall angular resolution of the detector, and the detector's geometric factor.

The geometric factor and number of particles that scattered at least once were calculated using the same simulation. An omnidirectional field was simulated by generating particles uniformly on a sphere with an angular distribution of $\cos^2 \theta$ where θ is the polar angle with respect to the sphere's normal vector and $0 \leq \theta \leq \pi/2$. The azimuthal angle was generated uniformly between 0 and 2π . Since these simulations are not focused on the shielding surrounding the detectors, simulation time was significantly reduced by only generating particles on a spherical cap positioned slightly above the entrance to the collimator. The cap was made large enough to ensure all possible angles of particles incident on the collimator were simulated. Based on this simulation set up the geometric factor (G) and its associated uncertainty can be calculated as

$$G = a \frac{n}{N} 4\pi r^2, \quad (1)$$

$$\sigma_G = a 4\pi^2 r^2 \left(\frac{n}{N^2} \left(1 - \frac{n}{N} \right) \right), \quad (2)$$

where n is the number of particles that are detected, N is the total number of particles, r is the radius of the sphere on which the particles are generated [16,17], and a is a scaling factor. The scaling factor is required since particles are generated only on the spherical cap and is calculated as

$$a = \frac{\text{Area of Cap}}{\text{Area of Sphere}}. \quad (3)$$

The cap is positioned such that all possible particles incident on the top of the collimator will be generated.

The number of particles which scatter before being detected is calculated based on whether the initial direction vector of the particle is the same as when the particle is incident on the first silicon detector. Additionally, the particle must deposit at least 5keV as this is the expected lower detection limit of the

first detector. The metric used for evaluating the design was the counting ratio, calculated as the total number of particles that entered the detector over the number of particles that underwent no scattering prior to detection. An ideal collimator would produce a ratio of one, while all non-ideal collimators will produce a ratio greater than one.

The angular resolution of the detector was determined by simulating large area beams of electrons in 5-degree intervals from 0 to 25 degrees. The calculated angle of incidence was determined by measuring the position of the particle incident on the first detector when more than 5keV was deposited. The incident angle is then calculated as

$$\theta = \tan^{-1} \frac{x}{l}, \quad (4)$$

where x is the position where the particle is incident on the detector ($x = 0$) is at the geometric center of the detector) and l is the distance from the detector to the collimator's aperture.

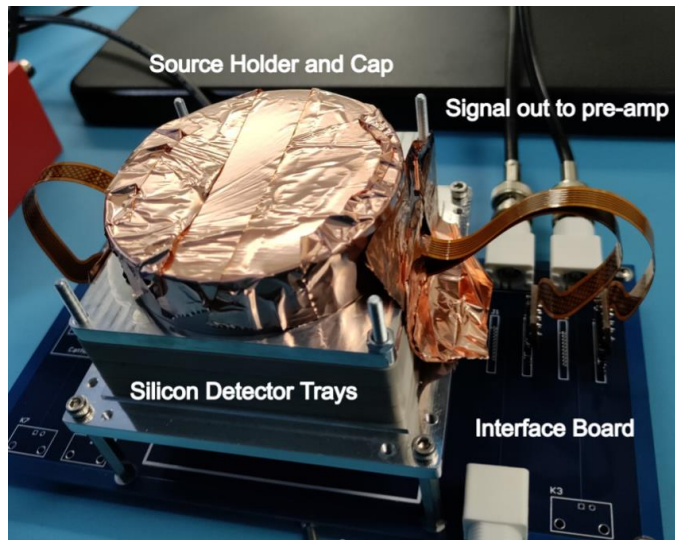


Figure 1: Test housing holding silicon detectors and source holder removed from vacuum chamber and Faraday cage.

IV. SIMULATION VERIFICATION

Verification of the simulations was accomplished using a testing system that could be simulated in Geant4 for result comparisons. The test system, shown in Figure 1, consists of two 1500 μm -thick MSD040 silicon detectors produced by Micron Semiconductors Ltd. The detectors are housed in a custom casing which contains an exchangeable source holder for testing. A breakout board was produced that allows the MSD040 detectors to convert its Omnetics connector to a BNC capable of interfacing with the preamplifiers. A CAEN preamplifier module (A1422) with a gain of 45 mV/MeV and a maximum detector capacitance of 1000pF were used and connected to a CAEN DT5724 digitizer. The CAEN preamps were powered using a CAEN DT5523 linear desktop power distributor. The signal between the preamplifier and digitizer were observed on an oscilloscope to ensure correct pulse shape and noise characteristics. High voltage was applied through the preamplifiers using a CAEN DT5534EP high-voltage power supply with a reverse bias voltage of 300V (full

depletion of the detectors occurred at 270V and 280V). When high voltage was applied a voltage ramp of 50V/s was used.

The test system was calibrated using a ^{244}Cm alpha source and a 140 μm -thick MSD040 silicon detector. The detector was placed in a vacuum chamber which was pumped down to 0.9 Torr to minimize energy loss before reaching the detector. The calibration was validated using a BNC Model PB-5 pulse generator in place of the silicon detector to ensure the system energy response was linear to within manufacturer standards.

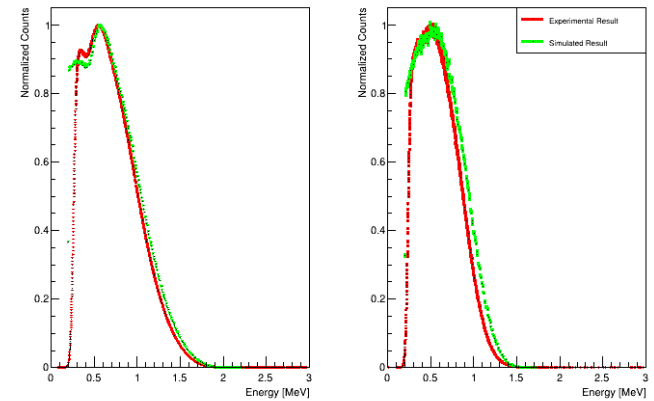


Figure 2: Experimental versus simulated spectrum from a $^{90}\text{Sr}/^{90}\text{Y}$ source incident on two 1500 μm -thick MSD040 silicon detectors in the test housing. First detector is on the left, second detector is on the right.

The test system was also placed in a light tight metal box acting as a faraday cage. A $^{90}\text{Sr}/^{90}\text{Y}$ source was placed in the source holder and the spectrum in both detectors was collected under atmospheric conditions. The experimental set up was simulated in Geant4 allowing comparisons between results shown in Figure 2. Both the simulation and experimental results have been normalized by their highest count and are rebinned to 10keV/bin to allow for easier comparison. Simulation results show good agreement with experimental data with all bins being within 5%. The largest discrepancy occurs at low energies where the simulation predicts lower counting rates than are observed by 5%. Drop off of detected electron below approximately 250keV can be seen and is caused by system noise making measurement of the lower energies impractical.

V. INSTRUMENT DESIGN

The design of the EST is constrained since it must fly on a 3U CubeSat. The total volume of the instrument is limited to 1U (10x10x10 cm³) and the mass should be minimized. Total power draw of the instrument will also need to be kept below 3W.

A. Collimator

A pin hole camera that allows particles to enter from within a cone was considered. While such a design allows a high geometric factor, the geometric factor as a function of pitch angle is not constant, reaching a minimum for pitch angles of 0 or 180 degrees. This design would therefore reduce the number of particles detected at the center of the loss cone. To

ensure the geometric factor remains constant across pitch angles, the aperture of the collimator was changed to a rectangle and the acceptance angle was limited to 5 degrees in

the y-axis and kept at 60 degrees in the x-axis. With such a design the geometric factor is constant across all pitch angles, however the geometric factor is severely limited.

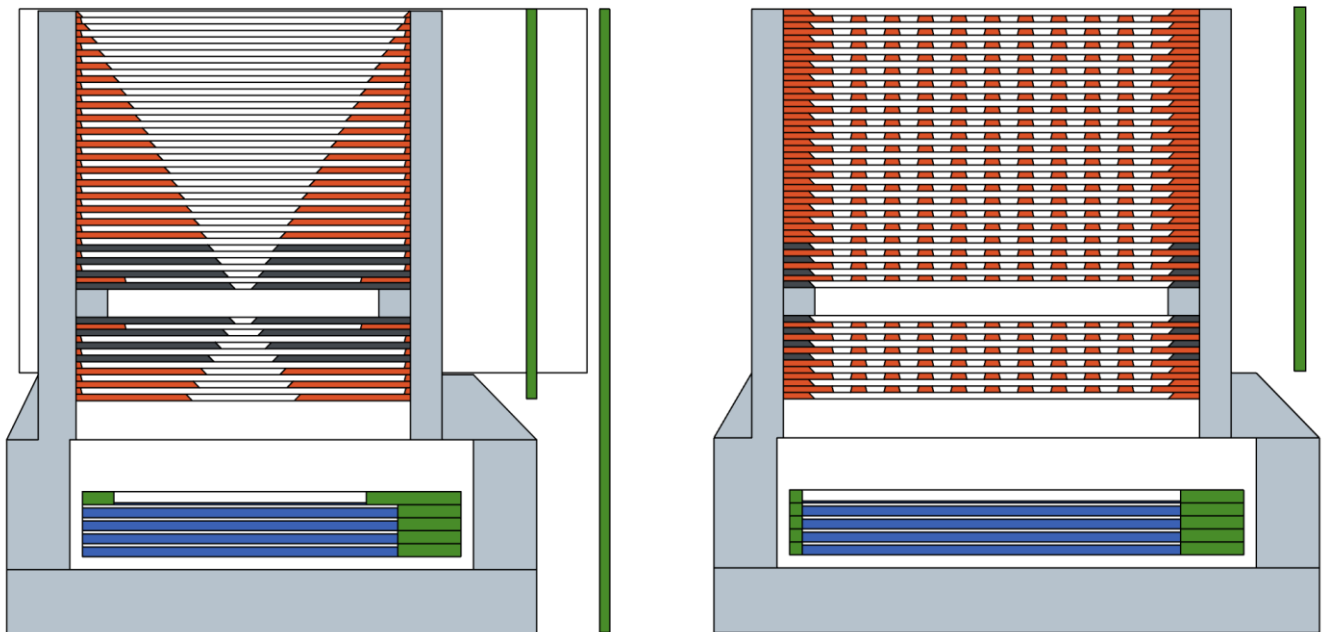


Figure 3: Cross-section views of the instrument in the x-z plane (left) and y-z plane (right). Materials are color coded as Green=FR4, Blue=Silicon, Light Grey = Aluminum, Dark Grey = Tungsten, Orange = Iron or Aluminum.

To solve the reduction in geometric factor, a new collimator design has been developed shown in Figure 3. The collimator is formed using two sets of alternating plates where one set of plates forms the converging-diverging shape of the pinhole camera while the second set of grating plates segment the trough shaped collimator into multiple smaller collimators with a y-axis acceptance angle of 5 degrees. Doing so results in increased the geometric factor linearly with the number of smaller collimators formed.

The collimator was designed by varying the length, width, height, material, and edge angle of the collimator plates. The total collimator length is restricted by the need to have a y-axis acceptance angle of 5 degrees. To achieve this the collimator is 60mm in height and each slit in the grating plates are 2.62mm in width resulting in a y-axis acceptance angle of 5.0006 degrees. The number of slits was then varied from 1 to 12 and it was noted that up to 10 slits can be positioned side by side before electrons begin entering the silicon stack after only one scattering event. The total y-axis length of the collimator is restrained to 66mm due to the 1U form factor and the need for support electronics. Therefore, with 8mm of shielding around the collimator the 10 slits result in 2.38mm of material between each slit.

The acceptance angle in the x-axis formed by the converging-diverging plates was predominantly driven by size constraints. Increasing the acceptance angle requires the first silicon detector to be positioned closer to the aperture of the collimator to ensure all electrons can be detected. However, the further away from the first detector is from the aperture the

larger the aperture can be for the same angular resolution. The silicon stack was placed 32mm from the aperture as this is the furthest possible without reducing performance of the collimator and staying within the volume constraints. These considerations make the largest possible acceptance angle 65 degrees, with the actual acceptance angle set as 60 degrees to allow for small modifications during manufacturing. Given the 32mm distance from the aperture to the first position sensitive silicon detector, the aperture width in the x-direction was maximized while maintaining acceptable angular resolution. The final aperture size is 2.50mm in the x-axis which when combined with the 10 slits, 2.62mm y-axis width, and 60-degree acceptance angle gives a geometric factor of $1.68(2) \times 10^{-2} \text{ cm}^2 \text{ sr}$.

The bevel angle on the plates was varied from 0 to 80 degrees in 5-degree increments. As expected, at a 0-degree bevel there is a significant increase in forward scattering resulting in many particles entering the silicon stack after a single scattering event. The collimator performance improved as the bevel angle of the converging-diverging plates was increased but remained fairly constant for angles between 35 and 50 degrees. Bevel angles above 50 degrees also began to decrease collimator performance due to particles penetrating through the much thinner material at the edge of the collimator. The grating plates could not have their bevel angle increased past 15 degrees since the reduction in material reduced the effectiveness of the 5-degree collimation. Therefore, the bevel angle of the grating plates is 15 degrees, and the bevel angle of the converging-diverging plates is 45

degrees.

Material choice for the collimator was limited to Aluminum, Tantalum, Tungsten, and Iron as the first three are materials often used for space born electron spectrometers and Iron is both easy to machine and readily available. It was noticed during simulations that there is no significant performance difference between Tantalum and Tungsten, therefore Tungsten was used for most simulations since it is the most likely material to be used in the final collimator. The best performance was provided by a fully Tungsten collimator providing a count ratio of 1.062(3) while the worst performance was provided by the fully aluminum collimator at a count ratio of 1.22(1). A fully Tungsten or Tantalum collimator would be impractical due to the mass budget, so

instead a combination of Aluminum and Tungsten plates was tested. It was found that grouping Tungsten plates together at the collimator aperture as seen in Figure 3 has the greatest effect on performance resulting in a counting ratio of 1.13(1). Adding additional tungsten or tantalum plates elsewhere in the collimator does improve performance slightly but at a significant increase in mass that cannot be accommodated. Changing the aluminum plates to Iron does significantly improve performance at a slight increase in mass resulting in a count ratio of 1.084(1). Both collimators with iron and aluminum will be tested before deciding on the final materials based on both total satellite mass budget and real-world collimator performance.

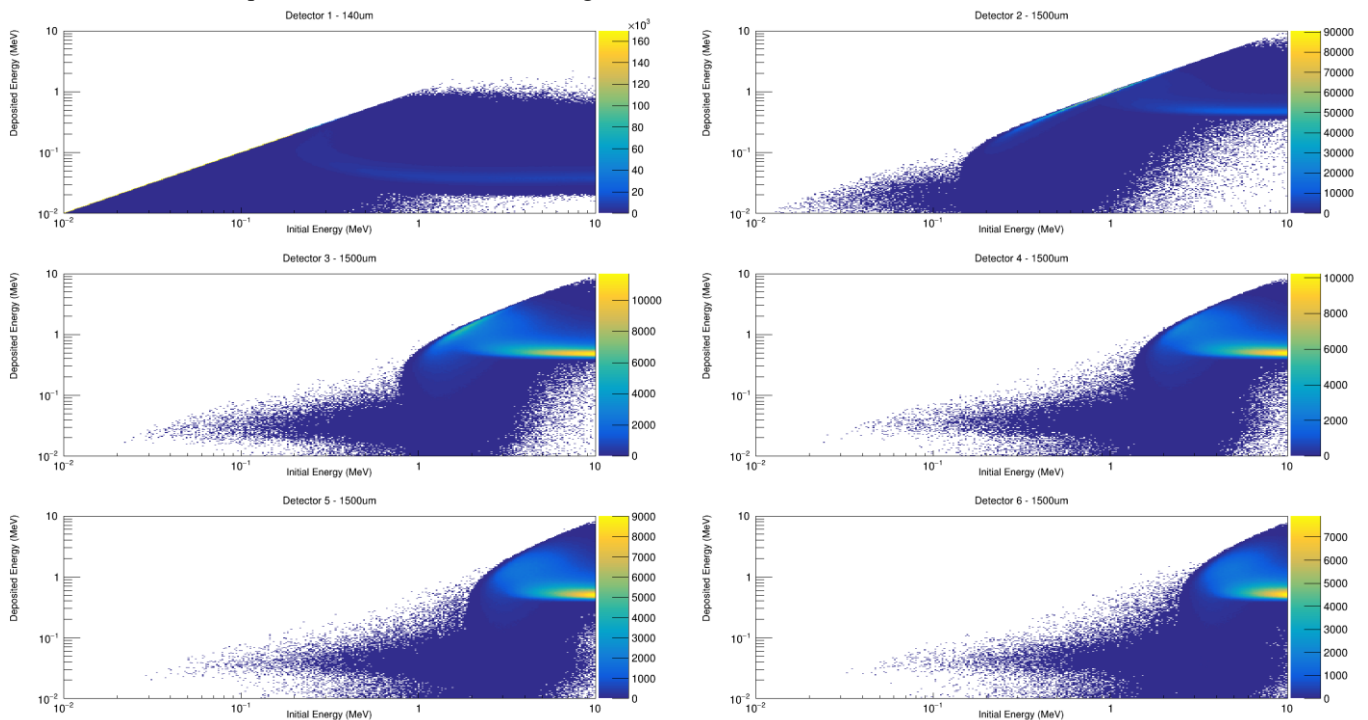


Figure 4: Response matrix of 6 Silicon detectors to electrons. Detector 1 is a 140um thick detector at the front of the detector stack while all other detectors are 1500um thick. Electron energies are distributed as such that each bin along the x-axis (initial energy) has the same number of initial particles. The color scale corresponds to the number of particles detected.

B. Silicon Stack

The silicon stack was simulated using a thin front detector followed by 4-7 1500-um thick detectors. The thick detectors were not adjusted as we intend to use the minimum number of detectors possible so the thickest available detectors will be used. The front thin detector will be used as both the initial trigger detector and will determine the position of the particle. The thin detector's thickness was simulated at 50 μm , 140 μm , 300 μm and 500 μm . Using the 300 μm and 500 μm detectors results in an average deposited energy of 110 ± 15 keV and 90 ± 10 keV respectively. Since the detector has no way to distinguish between an electron and a proton that fully deposit their energy in the first detector, minimizing the average energy deposited by a high energy electron will also lower the minimum detectable energy. The 140 μm and 50 μm detectors give an average deposited energy of 30 ± 10 keV and 15 ± 5

keV, both of which allow lower energy electrons to be distinguished from protons. The final design will use either a 50 μm or 140 μm detector depending on real world performance and manufacturability, with preference given towards the 50 μm detector.

The response matrix of the detector stack is shown in Figure 4 for a 140 μm thick front detector followed by five 1500 μm thick detectors. As expected, low energy electrons fully deposit their energy in the front detector while higher energy electrons deposit approximately 30 keV in the front detector. Electrons that pass through the first detector deposit either their entire remaining energy or between 400 keV to 900 keV in each subsequent detector until the electron has lost all energy or exited the detector stack. Electrons with initial energy below 4MeV typically deposit all their energy in the silicon stack while electrons with initial energy greater than 4

MeV fully penetrate the stack. Given the maximum energy deposited is approximately 4 MeV throughout the stack, the upper integral energy bin of the detector will be $E > 4 \text{ MeV}$. The final silicon stack will be composed of one 140 μm thick front detector followed by four 1500 μm thick detectors.

C. Instrument Performance

As previously mentioned, the geometric factor of the instrument is $1.68(2) \times 10^{-2} \text{ cm}^2 \text{ sr}$. The geometric factor can be converted to an expected counting rate using the SPENVIS AE-8 model [18]. Given a polar orbit between 400 and 500 km, the maximum expected counting rate at the poles is estimated to be 2500 Hz and the maximum counting rate in the South Atlantic Anomaly is estimated to be 9,500 Hz. These counting rates are comparable with previous space spectrometers and should be sufficient for producing useful data sets while not causing excessive dead time in the digital processing.

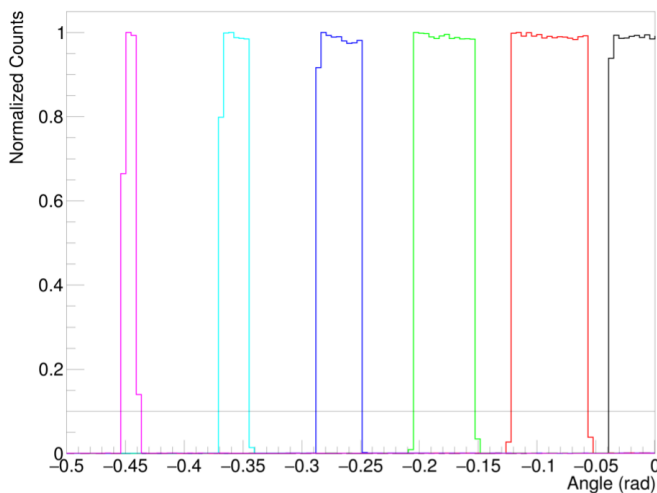


Figure 5: Simulated angular response of the EST to electrons with initial angles of 0, 5, 10, 15, 20, and 25 degrees.

Figure 5 shows the angular response of the instrument after removing particles that deposited less than 5 keV in the front detector, normalized by the highest bin counts per angle tested. Note that the angular response is symmetric about 0 degrees therefore the Figure 5 is plotted from -28 to 0 degrees. The particles used in the simulation follow the energy spectrum expected in a polar low earth orbit as extracted from SPENVIS [18]. Using the full width at 10% max gives an angular resolution of 4.5 degrees when the particle is normal to the detector stack and a resolution of 0.75 degrees when the particle is at the edge of the collimator acceptance angle. This performance significantly surpasses the requirement of 10-degree resolution; however it is expected that in real world testing, system noise will reduce the resolution causing the angular distribution to tend towards a Gaussian distribution.

VI. CONCLUSIONS

To measure electron pitch angle distribution in the Van Allen Belts a new electron spectrometer has been developed through simulation. Simulations were carried out in Geant4 allowing

the instrument geometry to be varied to produce an instrument with excellent performance. The new collimator design allows multiple pin hole camera's to be integrated into a single structure, reducing the number of silicon detector stacks required while providing a high geometric factor of $1.68(2) \times 1.68(s) \times 10^{-2} \text{ cm}^2 \text{ sr}$. The geometric factor translates to a maximum counting rate of approximately 2,500 Hz at the poles and 9,500 Hz in the South Atlantic Anomaly. The instrument contains a stack of 5 silicon detectors, with the first detector being either 50 μm or 140 μm in thickness and the following detectors each being 1500 μm thick. This results in a minimum detectable energy of 30keV and a maximum discernable energy of 4 MeV. Electrons with energies above 4 MeV will be placed in a high energy integral bin. Using a silicon strip detector with a pitch of 500 μm in conjunction with the collimator results in an angular resolution of 4.5 degrees. It is expected the angular resolution of the final instrument will be worse due to system noise, however it should stay well within the 10-degree resolution limit.

The next steps will be to fabricate the collimator plates out of iron, tungsten, and aluminum so different configurations of materials can be tested and the real-world detector performance can be evaluated. A vacuum system and electron gun are currently being developed to validate the instruments angular and energy resolutions. Custom electronics to process the raw signals and produce histogram data are currently under development and will be compared with the commercial system performance before integration into the PRESET satellite.

REFERENCES

- [1] National Academies of Sciences, Engineering, and Medicine, "Science discoveries and technical advances" in Progress Toward Implementation of the 2013 Decadal Survey for Solar and Space Physics: A Midterm Assessment, Washington, DC, USA: NAP, 2019, Ch.2, pp.34-48.
- [2] Zong, Q., Wang, Y., Yuan, C., Yang, B. Wang, C., and Zhang, X., "Fast acceleration of "killer" electrons and energetic ions by interplanetary shock stimulated ULF waves in the inner magnetosphere". *Chin.Sci.Bull.* **56**, 1188-1201 (2011)
- [3] Anderson, M.E., Verronen, P.T., Rodger, C.J., Clilverd, and M.A., Seppälä, A., "Missing driver in the Sun-Earth connection from energetic electron precipitation impacts mesospheric ozone. *Nat. Commum.* **5**, 5197 (2014)
- [4] Semeniuk, K., Fomichev, V.I., McConnell, J.C., Fu, C., Melo, S.M.L, and Usoskin, I.G., "Middle atmosphere response to the solar cycle in irradiance and ionizing particle precipitation." *Atm.Chem.and Phys.*, **11**(10), 5045-5077 (2011)
- [5] Codrescu, M.V., Fuller-Rowell, T.J., Roble, R.G., and Evans, D.S., "Medium energy particle precipitation influences on the mesosphere and lower thermosphere", *J. Geophys. Res.*, **102**, 19977-19987 (1997)
- [6] Arsenovic, P., Rozanov, E., Stenke, A., Funke, B., Wissing, J., Mursula, K., et al., "The influence of middle range energy electrons on atmospheric chemistry and regional climate. *J. Atmo. Sol.-Terr.Phys.*, **149**, 180-190 (2016)
- [7] Meraner, K., and Schmidt, H., "Climate impact of idealized winter polar mesospheric and stratospheric ozone losses as caused by energetic particle precipitation." *Atmo. Chem. and Phys.*, **18**(2), 1079-1089 (2018)
- [8] Tysøy, H.N., Haderlein, H.N., Sandanger, M.I., and Stadsnes, J., "Intercomparison of the POES/MEPED loss cone electron fluxes with the CMIP6 parametrization." *J. Geo.Phys. Res.Space.Phys.*, **124**, 628-642 (2019)
- [9] Tysøy, H.N., Sadanger, M.I., Ødegaard, L.-K.G., Standsnes, J., Aasnes, A., Zawedde, A.E., "Energetic electron precipitation into the middle atmosphere – Constructing the loss cone fluxes from MEPED POES." *J. Geo.Phys.Res.Space.Phys.*, **121**(6), 5693-5707 (2016)

- [10] Stratton, J.M., Harvey, R.J., and Heyler, G.A., "Mission Overview for the Radiation Belt Storm Probes Mission." *Space. Sci. Rev.*, **179**, 29-57 (2013)
- [11] Bakr, D.N., Kanekal, S.G., Hoxie, V., Li, X., Jaynes, A.N., Zhao, H., Elkington, S.R., *et al.*, "The relativistic Electron-Proton Telescope (REPT) Investigation: Design, Operational, Properties, and Science Highlights." *Space. Sci. Rev.*, **219**, 68 (2021)
- [12] Claudepierre, S.G., Blake, J.B., Boyd, A.J., Clemmons, J.H., Fennel, J.F., Gabrielse, C., *et al.*, "The Magnetic Electron Ion Spectrometer: A Review of On-Orbit Sensor Performance, Data, Operations, and Science." *Space Sci. Rev.*, **217**,80 (2021)
- [13] Mitani, T., Takashima, T., Kasahara, S., Miyake, W., Hirahara, M., "High-energy electron experiments (HEP) aboard the ERG (Arase) satellite." *Earth, Planets and Space.* **70**(77) (2018)
- [14] Kasahara, S., Miyoshi, Y., Yokota, S., Mitani, T., Kasahara, Y., Matsuda, S., *et al.*, "Pulsating aurora from electron scattering by chorus waves." *Nature*, **554**, 337-340 (2018)
- [15] Soti, G., Wauters, F., Breitenfeldt, M. Finlay, P., Kraev, I.S., Knecht, *et al.*, "Performance of Geant4 in Simulating Semiconductor Particle Detector Response in the Energy Range Below 1 MeV", *Nucl. Inst. Meth. Phys. Res. Sect. A*, **870**, 64-67 (2018)
- [16] Yando, K. Millan, R.M., Green, J.C., and Evans, D.S., "A Monte Carlo simulation of the NOAA POES Medium Energy Proton and Electron Detector instrument." *J.Geo.Phys.Res.*, **116**(A10231), (2011)
- [17] Sullivan, J.D., "Geometrical factor and directional response of single and multielement particle telescopes." *Nuc.Inst.Meth.*, **95**, 5-11 (1971)
- [18] Kruglanski, M., de Donder, E., Messios, N., Hetey, L., Calders, S., Evans, H., *et al.*, "Space Environment Information System (SPENVIS)" in *38th COSPAR Sci. Assem.*, Bremen, Germany, 2010, pp8